Modeling of O-18 tracer distribution during "double oxidation" experiments for inward growing scales

N. Appannagaari[a] and S. N. Basu[b]
Department of Manufacturing Engineering, Boston University, Boston, Massachusetts 02215

(Received 26 July 1994; accepted for publication 20 April 1995)

Quantitative modeling of oxygen tracer (^{18}O) concentration profiles obtained during double oxidation experiments has been carried out. An existing model in the literature, involving combined grain-boundary and lattice diffusion of oxygen with exchange, has been extended to cases where the grain size of the oxide is allowed to vary over its thickness. The model predicts tracer profiles in the entire oxide for the case of scale growth by inward oxygen diffusion. A computer program has been developed along with a graphical user interface for easy generation and visualization of simulated tracer profiles. The sensitivity of the simulated profiles to variations in volume (D^v) and grain-boundary (D^b) diffusivities of oxygen in the oxide scale as well as the oxide grain-size variation have been studied. The results indicate that the normalized tracer profiles are sensitive to variations in D^b, although to a lesser extent as compared to similar variations in D^v. Also, incorporation of variable grain size leads to profiles very different from those obtained from a constant oxide grain-size assumption. The computer program has been used to fit an experimental profile reported in the literature to obtain values of D^v and D^b. © *1995 American Institute of Physics.*

I. INTRODUCTION

The double oxidation technique is widely used to determine transport mechanisms in growing oxide scales.[1] This process consists of oxidation in natural ^{16}O to form an "old" oxide, followed by oxidation in ^{18}O (a naturally occurring isotope of oxygen which acts as a tracer) to form a "new" oxide. The relative location of the new oxide is then studied by surface analytical techniques such as secondary-ion mass spectrometry (SIMS). The resulting data can be used to obtain plots of ^{18}O concentration versus depth in the oxide, which can then be related to the transport mechanism. The qualitative shapes of the tracer concentration profile as a function of different dominant diffusion mechanisms that can occur in a growing oxide have been discussed by several authors.[2–4] However, as noted by Jedlinski, several considerations should be applied during interpretation of such profiles.[5]

Although the idea of interpreting the growth mechanism from the location of the new oxide is simple in principle, prediction of the actual shape of the profiles can be quite complex. This is due to the phenomenon of tracer "exchange" that occurs as a result of simultaneous grain-boundary and lattice diffusion in the oxide. Since grain-boundary diffusivity is typically substantially higher than bulk diffusivity, rapid diffusion of tracer along the oxide grain boundaries during tracer oxidation leads to differences in tracer concentration between the grains in the oxide and the grain boundaries that surround them. This leads to an exchange of natural and tracer oxygen atoms between grain boundaries and grains.

This phenomenon of combined inward grain-boundary and lattice oxygen diffusion with exchange was first mathematically modeled by Basu and Halloran,[2] assuming a spherical grain geometry, who predicted the shape of the tracer profiles in the old oxide as a function of oxygen diffusivities and oxide grain size. Wegener and Borchardt[6] improved upon this model to predict tracer profiles in the entire oxide, and showed that in certain limiting cases, the model agreed with well-known analytical solutions. This model was further extended by Bongartz and co-workers,[7] who showed that incorporation of a variable grain size led to improved fits to experimental data. However, this model assumed a linear variation of oxygen chemical potential in the presence of a variable grain size, which will be shown to be incorrect in this paper. It was also suggested by Quadakkers *et al.*[8] and later mathematically analyzed by Mishin and Borchardt[9,10] that the spherical grain geometry was not best suited at high oxidation temperatures (regime "A" in Harrison's[11] classification) and early stages of oxidation, due to the non-negligible contribution of volume diffusion in the growth of the oxides in these cases. Instead, a tetragonal or orthorhombic grain geometry was chosen in their models.

In the present paper, the spherical geometry of grains is retained due to the symmetry of the volume diffusion. This allows the exchange process to be treated as a 1D problem, which reduces the complexity of the numerical calculations. The spherical grain geometry is appropriate for Cr_2O_3[12] and Al_2O_3 scales at longer oxidation times and lower oxidation temperatures (regime "C" in Harrison's[11] classification), when the contribution of volume diffusion to oxide growth can be neglected. The original model of Basu and Halloran[2] has been extended to incorporate the effects of variable grain size in the oxide for the case of inward oxygen diffusion. The model predicts the tracer profile in the entire oxide. A graphical user interface has been developed for easy comparison of simulated and experimental profiles. It is recognized that the columnar grain morphology suggested by Mishin and Borchardt[9,10] leads to a more realistic physical picture for

[a]Currently at Ansoft Corporation, Pittsburgh, PA 15219.
[b]Corresponding author.

 0021-8979/95/78(3)/2060/10/$6.00

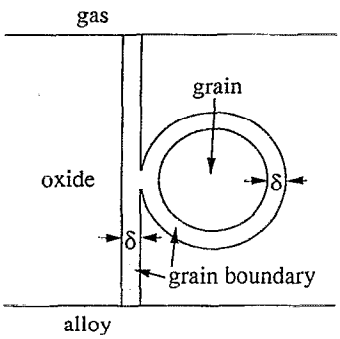

FIG. 1. Geometric configuration of oxide grain and grain boundary used in the model (partially after Oishi and Ichimura) (see Ref. 14).

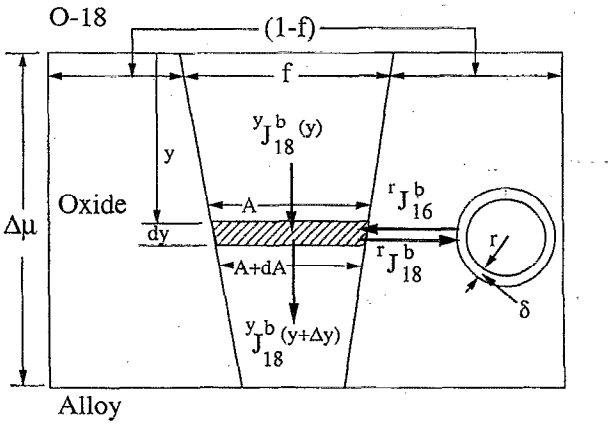

FIG. 2. Model of the variable cross-sectional area of the grain boundary (of area f) due to a variation in the grain size. The grains, whose strength depends on its grain size, act as sinks for ^{18}O and sources of ^{16}O. The grain boundary is modeled as a fast diffusion pipe which is continuously lined with sinks of variable strength. The figure also shows the fluxes in and out of a grain-boundary element of thickness dy, in the y and r directions.

NiO scales and Al_2O_3 scales[13] at short oxidation times. These cases would require simulation of 2D or even 3D diffusion processes, which are much more time intensive.

II. DIFFUSION MODEL

A. Model geometry

The current model retains the Oishi and Ichimura[14] geometric configuration of spherical grains as shown in Fig. 1. The model assumes that the rapid inward diffusion of oxygen tracer along the oxide grain boundaries (of thickness δ) dominates over volume diffusion through the grains, and is primarily responsible for new oxide growth (assuming very rapid lateral diffusion at the oxide/alloy interface). In this model, lattice diffusion contributes negligibly to the growth of the scale, but instead is responsible for an exchange of natural and tracer oxygen atoms between grain boundaries and grains, with the grains acting as sinks for ^{18}O and sources for ^{16}O.

For the chosen case of exclusively inward oxygen diffusion, the oxide is inward growing, with the total oxide thickness being a function of time defined as $Y(t)$. The origin of the y axis (normal to the oxide surface) is placed at the oxide/gas interface (see Fig. 2) and the grain radius variation as a function of depth is defined by a function $r(y)$. Although in principal, $r(y)$ (determined experimentally) can be any function, based on the experimental data by Bongartz *et al.*[7] for alumina scales (see Fig. 3), we will limit our case to a quadratic polynomial

$$r(y)=Ay^2+By+C, \tag{1}$$

where A, B, and C are constants. The model can easily be modified for higher-order polynomials. It is assumed that the diffusion processes during exchange can be modeled at any depth y by considering a spherical grain of radius $r(y)$ whose center is located at a depth y.

B. Oxygen diffusion through the scale

Oxygen diffuses from the gas to the oxide/alloy interface in response to a chemical-potential difference $\Delta\mu$. The total flux of oxygen through the oxide scale, j^{tot} (kg/m^2 s), has a grain boundary (j^b) as well as a volume (j^v) contribution, which can be written as

$$j^{\text{tot}}=fj^b+(1-f)j^v, \tag{2}$$

where f is the fraction of cross-sectional area occupied by grain boundaries, and can be calculated as

$$f=\frac{g\delta}{\lambda}, \tag{3}$$

where λ is the grain size ($=2r$) and g is a geometric factor which reflects the shape of the grain. For this model, centered at any depth y, is a grain of radius r. Associated with a grain is half the width of the grain boundary ($\delta/2$) surrounding it. Thus f can be approximated as

$$f=\frac{4\pi r^2\delta/2}{(4/3)\pi r^3+4\pi r^2\delta/2}\approx\frac{3\delta}{2r}\quad(\delta\ll r), \tag{4}$$

leading to $g\approx 3$.

Typically, for $\lambda\sim 1$ μm, $\delta\sim 1$ nm and $j^b/j^v\approx D^b/D^v\approx 10^4$ (D^b and D^v refer to grain-boundary and volume diffusivity of oxygen in the oxide), $fj^b/(1-f)j^v\approx 30$.

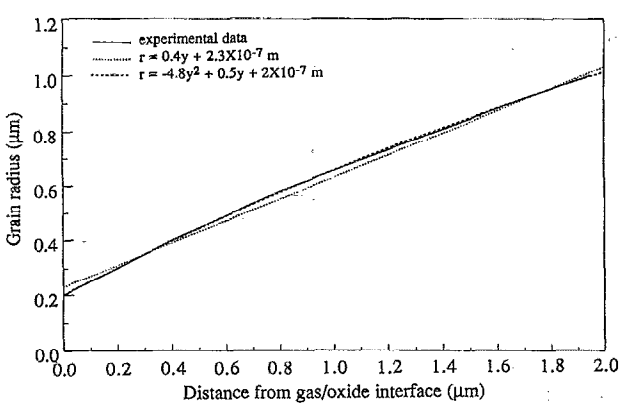

FIG. 3. Grain-size variation in Al_2O_3 scale, reported by Bongartz *et al.* (Fig. 4 in Ref. 7). The fit to a linear ($r=0.4y+2.3\times10^{-7}$ m) as well as a second-order polynomial ($r=-4.8y^2+0.4y+2\times10^{-7}$ m) variation with y is also shown in the figure.

This implies that grain-boundary diffusion is primarily responsible for the transport of oxygen (regime "C" in Harrison's classification) and that $j^{tot} \approx f j^b$. If the oxide (having a cross-sectional area A) increases in thickness by ΔY during oxidation for time Δt, the oxygen flux can be related to the oxygen concentration in the oxide, c^{tot} (kg of O/m^3 of oxide), by the following equation:

$$j^{tot} A \Delta t = \Delta Y A c^{tot}. \tag{5}$$

It should be noted that since most oxides used for oxidation resistance have low defect concentrations, they are stoichiometric (c^{tot} is constant). This means that diffusing oxygen atoms cannot accumulate within the scale, implying that the total oxygen flux j^{tot} is a function of time only and not of depth (i.e., at any given time, j^{tot} is constant throughout the thickness of the oxide).

The oxygen flux through the grain boundaries is driven by the gradient in the chemical potential of oxygen, and can be written as

$$j^b = -\frac{D^b}{RT}\frac{\partial \mu}{\partial y} c^{tot}, \tag{6}$$

where R and T are the universal gas constant and the oxidation temperature, respectively. It is assumed here that the diffusivities of ^{16}O and ^{18}O are the same. Combining Eqs. (2)–(6) and simplifying gives

$$\frac{\partial \mu}{\partial y} = -\frac{2RT}{g \delta D^b}\frac{dY}{dt} r. \tag{7}$$

It should be noted that for a constant grain size, the chemical-potential gradient in the scale, $\partial \mu / \partial y$, will be constant throughout the thickness of the scale at a given time, leading to the well-known parabolic growth law.[15] However, for a grain-size variation represented by Eq. (1), at any given time, Eq. (7) can be integrated through the thickness of the scale as

$$\int_{\mu_{oxide/gas}}^{\mu_{oxide/alloy}} d\mu = \Delta \mu = -\frac{2RT}{g \delta D^b}\frac{dY}{dt} \times \int_0^Y (Ay^2 + By + C)\, dy. \tag{8}$$

Since $\Delta \mu$ is a constant, Eq. (8) can be rearranged and further integrated as

$$\int_0^Y \left(\frac{AY^3}{3} + \frac{BY^2}{2} + CY\right) dY = -\frac{g \delta D^b}{2RT} \Delta \mu \int_0^t dt$$

$$\Rightarrow \frac{AY^4}{12} + \frac{BY^3}{6} + \frac{CY^2}{2} = -\frac{g \delta D^b}{2RT} \Delta \mu t. \tag{9}$$

Equation (9) shows that the oxide thickness $Y(t)$ is related to the grain-boundary diffusivity of oxygen, D^b. Thus D^b is not an independent variable and can be calculated from Eq. (9), if the grain-size variation (values A, B, and C) is known experimentally, and if the oxide thickness Y is known at any time t. We have used the thickness of the old oxide, $Y(\tau)$, after O-16 oxidation for time τ, to calculate the value of D^b.

Combining Eqs. (7) and (9), we can express the chemical-potential gradient of oxygen at any depth in the scale at any time as

$$\frac{\partial \mu}{\partial y} = \frac{r \Delta \mu}{(AY^3/3 + BY^2/2 + CY)}. \tag{10}$$

It should be noted that in Eq. (10) the depth information is implicit in the grain radius r, while the time information is implicit in the total oxide thickness Y. It is also interesting to note that for a variable grain size, the chemical-potential gradient is not constant. This is because as the fractional grain-boundary area changes with grain size, the oxide adjusts the chemical-potential gradient to ensure that at any time, the oxygen flux is constant at all depths within the scale.

C. Modeling of tracer diffusion

Having determined the variation in oxygen chemical-potential across the scale, it is now necessary to set up the diffusion equations for the transport of ^{18}O during the second stage of the double oxidation experiment. It is assumed that the old oxide formed during the first stage of oxidation consists entirely of ^{16}O. At this stage it is convenient to normalize flux j and oxygen concentration c by c^{tot} (kg of O/m^3 of oxide). This leads to a normalized flux J (m/s) and an unitless normalized oxygen concentration C.

The flux of ^{18}O down the grain boundaries (along the y axis), ${}^{y}J^b_{18}$,[16] is in response to two separate driving forces: a concentration gradient due to the presence of two oxygen species and a chemical-potential gradient as calculated in Eq. (10). This can be mathematically represented as

$${}^{y}J^b_{18} = -D^b \frac{\partial C^b_{18}}{\partial y} - \frac{D^b}{RT}\frac{\partial \mu}{\partial y} C^b_{18}. \tag{11}$$

In addition to the ^{18}O flux in the y direction, there is a flux of ^{18}O out of the grain boundary, ${}^{r}J^b_{18}$, and a corresponding equal and opposite flux ${}^{r}J^b_{16}$ into the grain boundary due to the exchange process. This is seen schematically in Fig. 2, which shows an oxide of unit cross-sectional area. The grain boundary, which is a rapid diffusion path, is shown as a pipe, having a variable cross-sectional area, defined by the function $f(y)$ [see Eq. (4)]. The grains act as sinks for ^{18}O, whose strength depends on their grain size. Thus the grain-boundary pipe in Fig. 2 is continuously lined with sinks of variable strength.

To consider the exchange process at each depth, a grain of radius $r(y)$ [see Eq. (1)] is surrounded by a grain boundary. Since grain-boundary diffusion of oxygen is considered to be fairly rapid, it is assumed that at any time the tracer concentration in a grain boundary surrounding a grain is the same throughout the grain boundary (this grain-boundary concentration does change with time). It is further assumed that the surface concentration of the grain is always the same as the concentration of the grain boundary surrounding it. Diffusion within the grain can then be defined by the well-known equation of diffusion in a sphere,[17]

$$\frac{\partial C_{18}^{\mathrm{grn}}}{\partial t}=D^{v}\left(\frac{\partial^2 C_{18}^{\mathrm{grn}}}{\partial \rho^2}+\frac{2}{\rho}\frac{\partial C_{18}^{\mathrm{grn}}}{\partial \rho}\right), \tag{12}$$

where ρ is the radial distance from the grain center and $C_{18}^{\mathrm{grn}}(\rho,t)$ is the normalized tracer concentration within a grain. The average tracer concentration within a grain at any time can thus be calculated as

$$C_{18}^{\mathrm{grn}}(\mathrm{avg})=\frac{\int_0^r 4\pi\rho^2 C_{18}^{\mathrm{grn}}\,d\rho}{(4/3)\pi r^3}. \tag{13}$$

Once a grain is formed, its tracer concentration can increase solely by the exchange process. Consider a small thickness dy in the scale (see Fig. 2). Let the average grain tracer concentration in depth dy increase by $\Delta C_{18}^{\mathrm{grn}}(\mathrm{avg})$ in time Δt. Since the number of oxygen sites in dy is constant, the mass of ^{18}O entering the grains due to exchange must be the mass of ^{18}O leaving the grain boundary (due to the exchange process only), leading to a tracer concentration decrease of ΔC_{18}^{b}. Since the areas of grain boundary and grains in dy is f and $(1-f)$, respectively, this mass balance can be written as

$$\Delta C_{18}^{\mathrm{grn}}(\mathrm{avg})(1-f)\Delta y=-\Delta C_{18}^{b} f\Delta y. \tag{14}$$

Thus the change in grain-boundary concentration with time due to the exchange process only can be written as

$$\frac{\partial C_{18}^{b}}{\partial t}=-\frac{(1-f)}{f}\frac{\partial C_{18}^{\mathrm{grn}}(\mathrm{avg})}{\partial t}. \tag{15}$$

One of the major advantages of the model we have chosen is that diffusion down the grain boundary and diffusion within a grain can both be individually treated as 1D problems (variables y and ρ, respectively). Strictly speaking, the flow through a pipe of variable cross section (see model of grain boundary in Fig. 2) cannot be 1D since there has to be a radial component of the flow. However, Fick's second law can be modified for a variable cross section to keep the problem 1D. Consider a portion of the grain boundary between y and $y+dy$ as shown in Fig. 2. The grain-boundary area at y is A and the entering flux is $J(y)$, while at $y+dy$, the area and flux are $A+dA$ and $J(y+dy)$, respectively. Due to the difference in incoming and outgoing fluxes, let there be a concentration change ΔC in time Δt. This can be mathematically written as

$$[J(y)A-J(y+\Delta y)(A+\Delta A)]\Delta t=\Delta C A\Delta y. \tag{16}$$

The incoming and outgoing fluxes can be related as

$$J(y+\Delta y)\approx J(y)+\Delta y\frac{\partial J(y)}{\partial y}. \tag{17}$$

Combining Eqs. (16) and (17) and simplifying gives

$$\frac{\partial C}{\partial t}=-J(y)\frac{1}{A}\frac{dA}{dy}-\frac{\partial J(y)}{\partial y}. \tag{18}$$

The first term on the right-hand side of the above equation accounts for the variable cross section and allows us to treat the grain-boundary diffusion as a 1D problem. Given that in our case the grain-boundary area A is defined as f, the diffusion of tracer in the grain boundaries with exchange can be written from Eqs. (15) and (18) as

$$\frac{\partial C_{18}^{b}}{\partial t}=-\frac{\partial {}^{y}J_{18}^{b}}{\partial y}-\frac{1}{f}\frac{df}{dy}{}^{y}J_{18}^{b}-\frac{(1-f)}{f}\frac{\partial C_{18}^{\mathrm{grn}}(\mathrm{avg})}{\partial t}. \tag{19}$$

The first two terms in the right-hand side of the above equation model grain-boundary diffusion through a variable cross section, while the third term accounts for the exchange process. Substituting into the above equation, the expressions for f and ${}^{y}J_{18}^{b}$ from Eqs. (4) and (11) give

$$\begin{aligned}\frac{\partial C_{18}^{b}}{\partial t}=&D^{b}\frac{\partial^2 C_{18}^{b}}{\partial y^2}+\frac{D^{b}}{RT}\frac{\partial \mu}{\partial y}\frac{\partial C_{18}^{b}}{\partial y}+\frac{D^{b}}{RT}\frac{\partial^2 \mu}{\partial y^2}C_{18}^{b}\\&-D^{b}\frac{1}{r}\frac{dr}{dy}\frac{\partial C_{18}^{b}}{\partial y}-\frac{D^{b}}{RT}\frac{1}{r}\frac{dr}{dy}\frac{\partial \mu}{\partial y}C_{18}^{b}\\&-\frac{(1-f)}{f}\frac{\partial C_{18}^{\mathrm{grn}}(\mathrm{avg})}{\partial t}.\end{aligned} \tag{20}$$

Thus the variation of tracer concentration within the grain boundaries and grains is described by Eqs. (20) and (12), respectively. Having solved Eqs. (12) and (20) for the grain and grain-boundary tracer concentration, the overall tracer concentration (which is what is experimentally measured) $C_{18}^{\mathrm{tot}}(y,t)$ can then be calculated as

$$C_{18}^{\mathrm{tot}}(y,t)=fC_{18}^{b}+(1-f)C_{18}^{\mathrm{grn}}(\mathrm{avg}). \tag{21}$$

D. Boundary conditions

Equations (12) and (20) need to be solved using the following boundary conditions:

(a) The oxide formed during the first stage of oxidation (old oxide) is all ^{16}O:

$$C_{18}^{b}|_{t=\tau,y}=C_{18}^{\mathrm{grn}}|_{t=\tau,y,0\leq\rho\leq r}=0. \tag{22}$$

(b) The oxygen flux entering the oxide at the gas/oxide interface during the second stage of oxidation is through the grain boundaries only and is all ^{18}O. Consequently, the grain-boundary ^{16}O flux at the oxide free surface during the second stage of oxidation is zero:

$${}^{y}J_{16}^{b}|_{t\geq\tau,y=0}=0. \tag{23}$$

(c) The surface tracer concentration of a grain is always equal to the concentration of the grain boundary surrounding it:

$$C_{18}^{\mathrm{grn}}|_{t,y,\rho=r}=C_{18}^{b}|_{t,y}. \tag{24}$$

(d) The concentration of the last grain-boundary element (at the oxide/alloy interface) does not change with time. The composition of this element begins to change when it is no longer the last element due to the addition of a new element. If the last grain-boundary element is formed at time T, and remains a last element up to time $T+\Delta T$,

$$C_{18}^{b}|_{T\leq t\leq T+\Delta T,y=Y}=\text{constant}. \tag{25}$$

(e) At time T, when a new element is added at $Y+\Delta Y$ (representing oxide growth at the oxide/alloy interface), the

grain and grain-boundary concentration at the newly formed element is equal to that of the previous grain-boundary element at time T:

$$C_{18}^{b}|_{t=T,y=Y+\Delta Y}=C_{18}^{\mathrm{grm}}|_{t=T,y=Y+\Delta Y,0\leq\rho\leq r}=C_{18}^{b}|_{t=T,y=Y-\Delta Y}. \tag{26}$$

(f) Due to symmetry, the flux at the center of a grain is zero:

$$\left.\frac{\partial C_{18}^{\mathrm{grm}}}{\partial\rho}\right|_{t,y,\rho=0}=0. \tag{27}$$

E. Numerical technique

Equations (12) and (20) have been numerically solved by the finite difference method. The forward time and forward space scheme has been used for Eq. (20), which upon discretization into space elements (i) and time elements (j) yields

$$C_{18}^{b}(i,j+1)=A'C_{18}^{b}(i+1,j)+B'C_{18}^{b}(i,j)+C'C_{18}^{b}(i-1,j)+D', \tag{28}$$

where

$$A'=\frac{D^b\Delta t}{(\Delta y)^2}+\frac{D^b\Delta t}{\Delta y}\frac{1}{RT}\frac{\partial\mu}{\partial y}-\frac{D^b\Delta t}{\Delta y}\frac{1}{r}\frac{dr}{dy},$$

$$B'=1-\frac{2D^b\Delta t}{(\Delta y)^2}-\frac{D^b\Delta t}{\Delta y}\frac{1}{RT}\frac{\partial\mu}{\partial y}+\frac{D^b\Delta t}{RT}\frac{\partial^2\mu}{\partial y^2}+\frac{D^b\Delta t}{\Delta y}\frac{1}{r}\frac{dr}{dy}-\frac{D^b\Delta t}{RT}\frac{\partial\mu}{\partial y}\frac{1}{r}\frac{dr}{dy},$$

$$C'=\frac{D^b\Delta t}{(\Delta y)^2},$$

$$D'=-\frac{(1-f)}{f}\{C_{18}^{\mathrm{grm}}(\mathrm{avg})[1,j+1]-C_{18}^{\mathrm{grm}}(\mathrm{avg})[i,j]\}.$$

It should be noted that D' in the above equation includes the term $C_{18}^{\mathrm{grm}}(\mathrm{avg})[i,j+1]$, which is calculated using the tracer concentrations at discrete grid points within the grain. Since the surface concentration of the grain is always taken to be equal to the grain-boundary tracer concentration at that depth [Eq. (24)], calculation of the term D' requires $C_{18}^{b}(i,j+1)$ to be known. Thus Eq. (28) has $C_{18}^{b}(i,j+1)$ in the right-hand side also, and needs to be solved iteratively. This is achieved by assuming a value for the grain-boundary concentration and going into an infinite loop until the calculated and assumed values coincide within a chosen tolerance (<1% error).

In order for the convergence of the numerical calculations required to solve Eq. (28), the space and time increments Δy and Δt are limited by the following equations:

$$\Delta y<\left(\frac{1}{r}\frac{dr}{dy}-\frac{1}{RT}\frac{d\mu}{dy}\right)^{-1},$$

$$\Delta t<\left(\frac{2D^b}{(\Delta y)^2}+\frac{D^b}{\Delta y}\frac{1}{RT}\frac{\partial\mu}{\partial y}-\frac{D^b}{RT}\frac{\partial^2\mu}{\partial y^2}-\frac{D^b}{\Delta y}\frac{1}{r}\frac{dr}{dy}+\frac{D^b}{RT}\frac{\partial\mu}{\partial y}\frac{1}{r}\frac{dr}{dy}\right)^{-1}. \tag{29}$$

To solve Eq. (12), the transformation $u=C_{18}^{\mathrm{grm}}\rho$ has been used, which reduces Eq. (12) to

$$\frac{\Delta u}{\partial t}=D^v\frac{\partial^2 u}{\partial\rho^2}. \tag{30}$$

The boundary conditions for Eq. (12) are also appropriately transformed and the equation is then solved by the standard forward time centered space scheme. Upon discretization into space elements in the radial direction (k) and time elements (j), Eq. (30) is reduced to

$$u(k,j+1)=E'u(k+1,j)+F'u(k,j)+G'u(k-1,j), \tag{31}$$

where

$$G'=E'=\frac{D^v\Delta t}{(\Delta\rho)^2},\quad F'=1-\frac{2D^v\Delta t}{(\Delta\rho)^2}.$$

For convergence, the conditions are

$$\Delta t\leq\frac{(\Delta\rho)^2}{2D^v},\quad \Delta\rho>0. \tag{32}$$

For the solution of the complete problem, when Eqs. (28) and (31) are solved simultaneously, Δt is chosen to be the smaller of the two values predicted by Eqs. (29) and (32). In general, the space increments (Δy and $\Delta\rho$) are of the order of 10^{-8} m, while the time increments are of the order of 2 s.

F. User interface

A graphical, easy to use, user interface has been developed[18] using the motif widget set to facilitate data management and generation and visualization of the tracer profiles. The two main objects of the interface are (i) the control panel and (ii) the graph. The control panel allows for the creation and deletion of input files that contain independent parameters such as diffusivities, radius variation, oxidation times, etc. A calculate option allows for the tracer concentration data to be generated from these files with the storage and retrieval of the generated data being abstracted from the user. Tracer concentration data corresponding to different input files can be independently generated in parallel on different workstations, thereby reducing calculation times. A plot option in the control panel also generates a graph object corresponding to the selected input file, such that the tracer profiles can be visualized.

The graph object allows plots to be visualized at any stage of the calculation (without interrupting the calculations), thereby allowing the user to follow the development of the final profile (e.g., for a total tracer oxidation of 30 h, at a time when calculations for 10 h of tracer oxidation is complete, it is possible to plot the profile at any time between 0

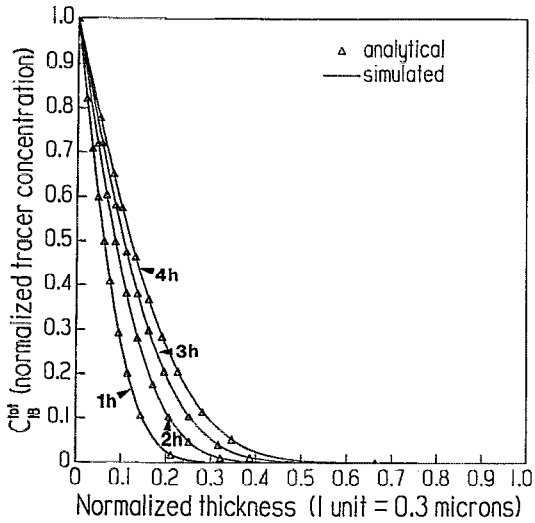

FIG. 4. Test case of volume diffusion without a chemical-potential gradient. The conditions chosen are $\Delta\mu=0$, $f=1$ ($r=3\times10^{-7}$ m, $\delta=2\times10^{-7}$ m), $D^v=0$, $D^b=10^{-19}$ m^2/s, $\tau=1$ h, and $t-\tau=1$, 2, 3, and 4 h. The figure shows that the simulated profiles are indistinguishable from the analytical solution.

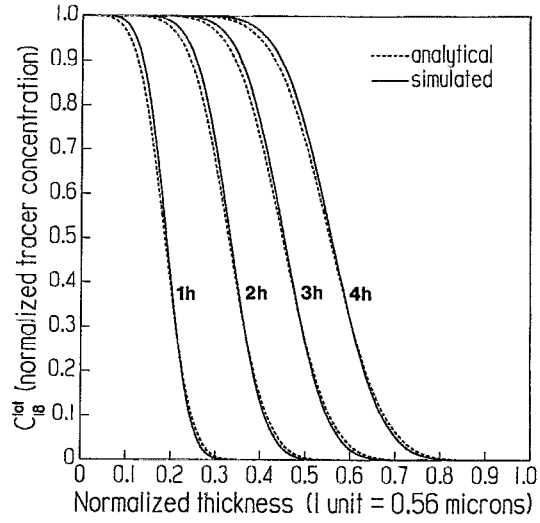

FIG. 5. Test case of volume diffusion in the presence of a chemical-potential gradient. The conditions chosen are $\Delta\mu=10^6$ J/mol, $f=1$ ($r=3\times10^{-7}$ m, $\delta=2\times10^{-7}$ m), $D^v=0$, $D^b=10^{-19}$ m^2/s, $\tau=1$ h, and $t-\tau=1$, 2, 3, and 4 h. The figure shows a close match between the simulated profiles (bold lines) and the analytical solution (dotted lines).

and 10 h of tracer oxidation by setting a scroll bar to the desired time). The graph object also allows for superposition of plots, which is important if a match between experimental and calculated data is sought. It is thus possible to display the experimental data on the screen and superimpose profiles from different input files to obtain the best fit. The visualized plots can then be sent to a postscript printer.

III. RESULTS

A. Test cases

As suggested by Wegener and Borchardt,[6] we have run some test cases to ascertain the accuracy of our rather complex computer program. The first case treated is that of pure volume diffusion of tracer during the second oxidation stage into an O-16 scale [grown for 1 h (τ) during the first oxidation stage], in the absence of a chemical-potential gradient ($\Delta\mu=0$). For this simulation, we have chosen conditions similar to those reported by Wegener and Borchardt,[6] i.e., $f=1$ ($r=3\times10^{-7}$ m, $\delta=2\times10^{-7}$ m), $D^v=0$ (no sinks), and D^b ($=D^v$)$=10^{-19}$ m^2/s. This allows the grain boundary to be treated as a "volume" of constant cross-sectional area with no sinks, a situation which has a simple analytical solution given by[6]

$$C_{18}^{tot}(y,t)=C_{18}^{tot}(y=0,t)\,\mathrm{erfc}\left(\frac{y}{2[D^v(t-\tau)]^{1/2}}\right), \qquad (33)$$

where $C_{18}^{tot}(y=0,t)$ is the surface tracer concentration during tracer oxidation ($=1$). Figure 4 shows that the simulated profiles (for $t-\tau=1$, 2, 3, and 4 h) are indistinguishable from the analytical solution.

We have also carried out the volume diffusion test in the presence of a chemical-potential gradient. The conditions chosen are the same as above with the exception that $\Delta\mu=10^6$ J/mol. Figure 5 shows a comparison of the simulated profiles with those generated from the approximate analytical solution[6]

$$C_{18}^{tot}(y,t)=\frac{C_{18}^{tot}(y=0,t)}{2}\times\mathrm{erfc}\left(\frac{y-(2D^v\Delta\mu/RT)^{1/2}(t^{1/2}-\tau^{1/2})}{2[D^v(t-\tau)]^{1/2}}\right). \qquad (34)$$

Figure 5 shows that the match between the simulated and calculated profiles are not exact. As explained in detail by Wegener and Borchardt,[6] this is due to the approximation made in the boundary condition at the gas/oxide interface while deriving the analytical solution. Given the small error in the analytical solution, the close match between the plots in Fig. 5 and the complete match between the plots in Fig. 4 validate the accuracy of our computer program.

B. Simulated tracer profiles

Tracer concentration profiles have been generated using the computer program in order to study their sensitivity to variations in independent parameters such as lattice and grain-boundary diffusivities as well as grain size distribution. In all cases, the grain-boundary thickness δ has been assumed to be 1 nm, while the oxygen chemical-potential difference between the oxide/alloy and the oxide/gas interfaces is taken to be -789 kJ/mol at 1100 °C.[2] To determine grain-size variation, the experimental data reported by Bongartz and co-workers[7] (reproduced here in Fig. 3) has been used. Figure 3 shows that the grain-size variation is almost linear. The values of the constants in the grain-size equation [Eq. (1)] are chosen as $A=0$, $B=0.4$, and $C=2.3\times10^{-7}$ m, and the plot of the linear equation is shown in Fig. 3. The oxida-

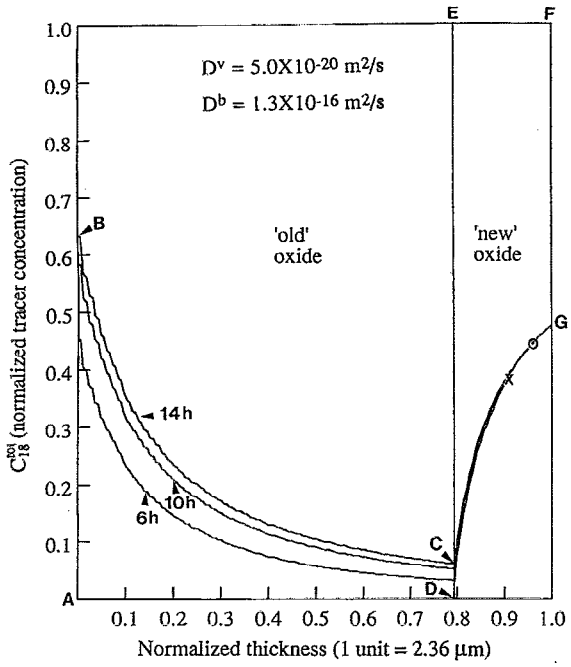

FIG. 6. Development of tracer concentration profiles with time. The conditions chosen are $D^b=1.3\times10^{-16}$ m^2/s, $D^v=5.0\times10^{-20}$ m^2/s, $\tau=18$ h, and $t-\tau=6$, 10, and 14 h. The total oxide thickness after 6 and 10 h of tracer oxidation is marked by x and o, respectively. Area $ABCD$ (amount of ^{18}O in the old oxide after 14 h of tracer oxidation) is equal to area $CEFG$ (amount of ^{16}O in the new oxide).

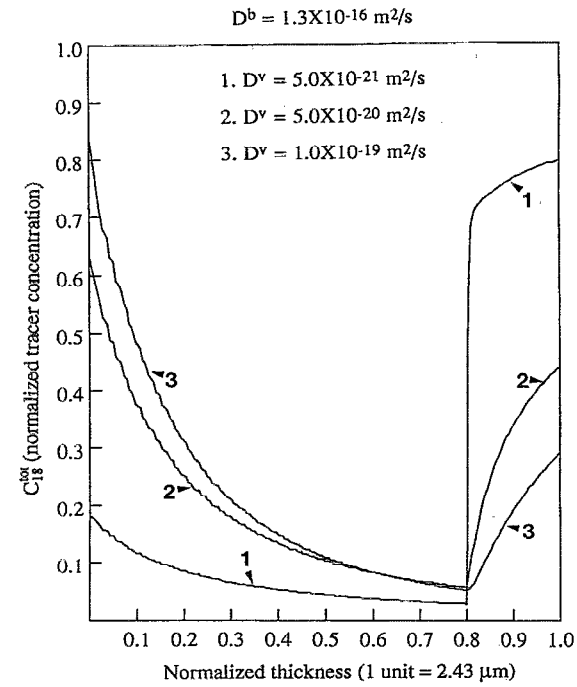

FIG. 7. Effect of varying D^v on tracer concentration profiles. The conditions chosen are $D^b=1.3\times10^{-16}$ m^2/s, $\tau=18$ h, $t-\tau=14$ h, and $D^v=5.0\times10^{-21}$, 5.0×10^{-20}, and 1.0×10^{-19} m^2/s.

tion times for the first and second stages of the double oxidation experiment are chosen as 18 and 14 h, respectively.

Figure 6 shows the development of the tracer concentration profile after tracer oxidation times of 6, 10, and 14 h for $D^b=1.3\times10^{-16}$ m^2/s and $D^v=5.0\times10^{-20}$ m^2/s and $\tau=18$ h. The total oxide thickness after 6 and 10 h of tracer oxidation is marked by x and o, respectively, in the figure. The figure shows that tracer profile in the old oxide undergoes a significant increase with time, while the change of the profile in the new oxide is mostly due to oxide growth (i.e., the effect of exchange in the new oxide is negligible). This is attributed to the fact that the tracer concentration difference between the grain and grain boundaries is much larger in the old oxide as compared to the new oxide. It should also be noted that, in our model, since the second oxidation is carried out in pure ^{18}O, any ^{16}O atom in the new oxide had to come from the exchange process. Since the number of oxygen sites per unit volume of the oxide is fixed, the number of ^{18}O atoms in the old oxide must equal the number of ^{16}O atoms in the new oxide. This implies that the area under the tracer concentration profile in the old oxide (area $ABCD$ in Fig. 6) must equal to the area over the profile in the new oxide (area $CEFG$ in Fig. 6). This criteria is satisfied in all plots generated by our computer program, further confirming its veracity.

Figure 7 shows the variation of the tracer concentration profile, when the value of D^b is fixed (1.3×10^{-16} m^2/s), and the value of D^v is varied (5.0×10^{-21}, 5.0×10^{-20}, and 1.0×10^{-19} m^2/s). The plots show that increasing D^v increases the strength of the sink term, thereby allowing for a larger concentration of ^{18}O to be retained in the old oxide, while decreasing the tracer content of the new oxide. This in turn reduces the sharpness of the tracer profile at the old oxide/new oxide interface. Thus the major role of volume diffusivity is to dilute the tracer content of the grain boundaries in the old oxide.

Figure 8(a) shows the effect of varying D^b (5.0×10^{-17}, 1.3×10^{-16}, and 5.0×10^{-16} m^2/s), at a constant value of D^v (5.0×10^{-20} m^2/s). The plots, which have been normalized to the final thickness of the fastest growing scale, show the effect of D^b on the growth rate of the oxide. As expected, increasing D^b increases the flux of ^{18}O from the atmosphere into the oxide grain boundaries during tracer oxidation, thereby enhancing the exchange process. Figure 8(b) shows the same plots normalized to their individual old oxide thickness. The plots show that the normalized tracer profiles are less sensitive to variations in D^b (compared to similar variations in D^v), in agreement to the observations of Wegener and Borchardt.[6] However, unlike in their case, where they had an exact match of all profiles with varying D^b in the old oxide, our plots do show an effect of D^b variation. This is mainly because Wegener and Borchardt considered a constant oxide grain-size case, which led to parabolic growth kinetics. They then proved mathematically that the normalized profiles should be insensitive to D^b variations. This proof does not hold true in our case, since the variation in the oxide grain size leads to nonparabolic growth kinetics. Interestingly, Fig. 8(b) shows that an increase in D^b leads to a *decrease* in the normalized tracer concentration profile in the old oxide. We attribute this to a competition between faster tracer diffusion through the grain boundaries of the old oxide (thereby increasing the tracer concentration profile in the old

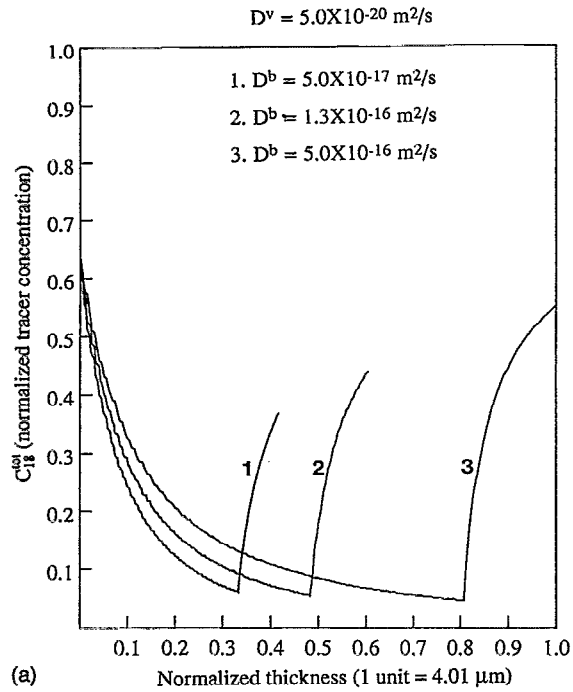

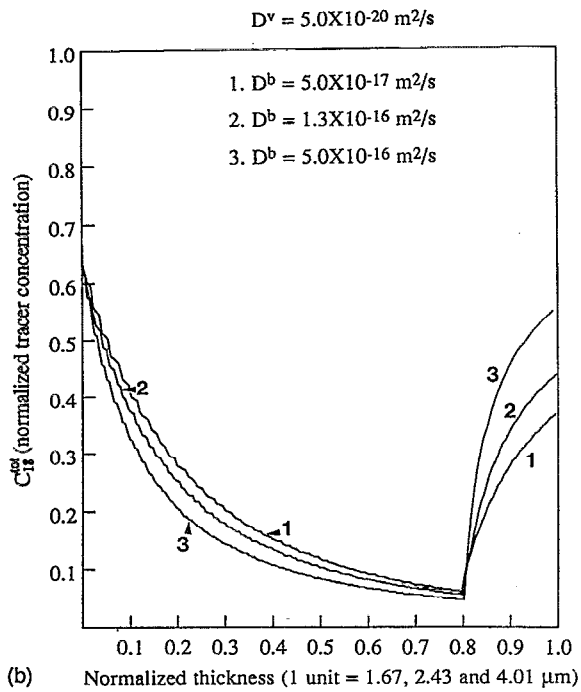

FIG. 8. (a) Effect of varying D^b on tracer concentration profiles. The conditions chosen are $D^v=5.0\times10^{-20}$ m^2/s, $\tau=18$ h, $t-\tau=14$ h, and $D^b=5.0\times10^{-17}$, 1.3×10^{-16}, and 5.0×10^{-16} m^2/s. (b) Plots in (a) normalized to their individual old oxide thickness.

oxide) and larger diffusion distances due to enhanced oxide growth rates (thereby decreasing the tracer concentration profile), with the latter phenomenon prevailing. Of course, the actual *amount* of tracer retained in the old oxide increases with increasing D^b [Fig. 8(a)].

The effect of grain-size variation on the tracer concentration profiles is illustrated in Fig. 9. The figure shows su-

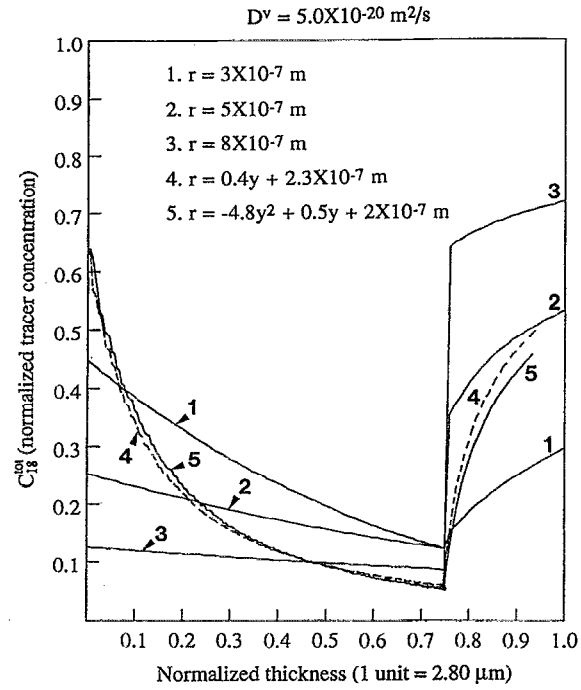

FIG. 9. Effect of varying r on tracer concentration profiles. The conditions chosen are $D^v=5.0\times10^{-20}$ m^2/s, $\tau=18$ h, $t-\tau=14$ h, and r as constant (3×10^{-7}, 5×10^{-7}, and 8×10^{-7} m), linear in y ($0.4y+2.3\times10^{-7}$ m) and second-order polynomial of y ($-4.8y^2+0.4y+2\times10^{-7}$ m). The D^b value has been adjusted such that the old oxide thickness is the same in all cases.

perimposed tracer concentration plots for a linear ($r=0.4y+2.3\times10^{-7}$ m) as well as a second-order polynomial of y [$A=-4.8$ m^{-1}, $B=0.5$, and $C=2.0\times10^{-7}$ m in Eq. (1); see Fig. 3] fit to the grain-size variation data reported by Bongartz *et al.*,[7] along with plots for constant grain radii of 0.3, 0.5, and 0.8 μm, respectively. The D^v value of 5.0×10^{-20} m^2/s has been used for the plots, while the D^b value has been adjusted such that the old oxide thickness is the same in all cases. The figures show that, as suggested by Bongartz *et al.*,[7] incorporation of variable grain size leads to profiles that are very different from those obtained from a constant grain-size assumption. Comparison of the profiles of constant grain size reveals that smaller grain sizes lead to enhanced exchange due to the larger grain-boundary surface area available. Among the two profiles of variable grain size, since the experimentally measured grain size is almost linear, a quadratic polynomial fit of the experimentally observed data does not lead to a significantly different profile. However, the smaller grain size near the oxide/gas interface, obtained by the second-order polynomial fit, leads to an increased tracer concentration profile (compared to the linear case) due to enhanced tracer exchange in the top part of the oxide (close to oxide/gas interface).

We have used our computer program to fit experimental profiles reported by Bongartz *et al.*[7] for the oxidation of Fe-CrAl based oxide dispersion strengthened alloys at 1100 °C. Bongartz *et al.* reported the tracer concentration profile for a MA956 alloy [Fe–20(wt %)Cr–4.5Al–0.3Ti–0.5Y_2O_3] oxi-

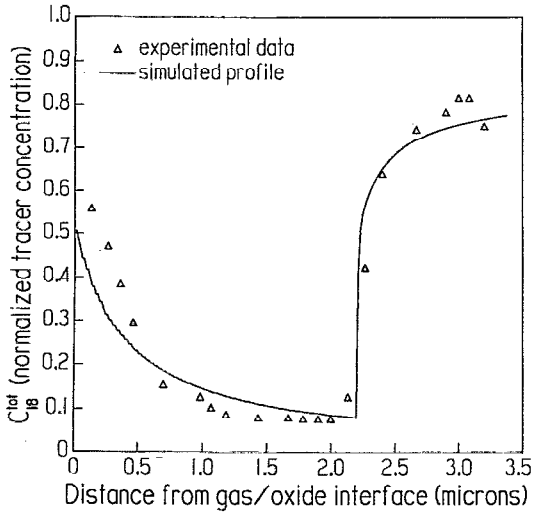

FIG. 10. Fit to experimental data reported by Bongartz *et al.* (Fig. 7 in Ref. 7) for the oxidation of a Fe–20Cr–4.5Al–0.3Ti–0.5Y_2O_3 alloy at 1100 °C for times of 75 and 150 h in ^{16}O and ^{18}O, respectively. The figure shows our best fit simulated plot for $D^v=3.0\times10^{-21}$ m^2/s and $D^b=5.0\times10^{-17}$ m^2/s and the grain-size variation reported by the same authors.

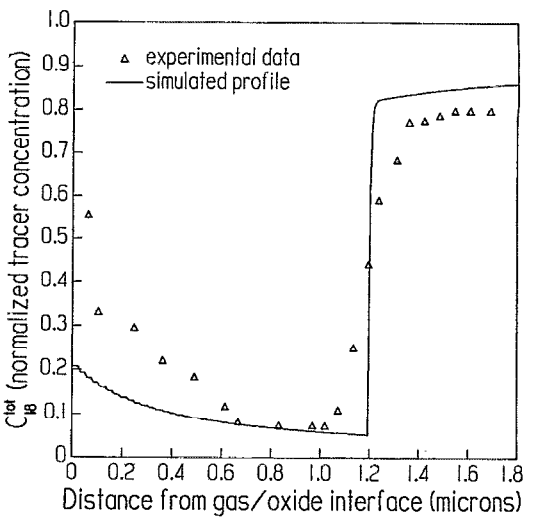

FIG. 11. Fit to experimental data reported by Bongartz *et al.* (Fig. 11 in Ref. 7) for the oxidation of a Fe–20Cr–5.5Al–0.3Ti–0.5Y_2O_3 alloy at 1100 °C for times of 15 and 30 h in ^{16}O and ^{18}O, respectively, using the same D^v and D^b values (3.0×10^{-21} and 5.0×10^{-17} m^2/s, respectively) and grain-size variation used for the fit in Fig. 10.

dized at 1100 °C for times of 75 and 150 h in ^{16}O and ^{18}O, respectively. Figure 10 shows the fit between the experimental data and our simulated plot for $D^v=3.0\times10^{-21}$ m^2/s and $D^b=5.0\times10^{-17}$ m^2/s and a grain-size variation reported by the same authors.[7] To our knowledge, this is the only case in which tracer profiles and grain-size variations have been reported simultaneously. Figure 10 shows that the fit between the simulated and experimental profiles is not exact. This is not surprising, given the complicated nature of the diffusion processes involved, as well as the limitations of the SIMS observations. Although the exact cause of the discrepancy is hard to pinpoint, possible factors may be speculated on. These include nonuniform sputtering of grains and grain boundaries during SIMS observations, nonuniform segregation of yttrium ions in the oxide from Y_2O_3 precipitates, leading to variable volume diffusivities in the oxide, and grain growth during oxidation, among others.

Bongartz and co-authors also reported experimental tracer profiles for shorter oxidation periods at 1100 °C (15 and 30 h of ^{16}O and ^{18}O oxidation, respectively) for a PM2000 alloy, which is very similar to MA965 in composition [Fe–20(wt %)Cr–5.5Al–0.3Ti–0.5Y_2O_3]. Figure 11 shows the fit between the experimental data and our simulated plot for the PM2000 alloy, using the same values of diffusivities ($D^v=3.0\times10^{-21}$ m^2/s and $D^b=5.0\times10^{-17}$ m^2/s) and a grain-size variation. It can be seen that the fit to the shorter oxidation time case in Fig. 11 is not as good as that of the longer oxidation time case in Fig. 10.

IV. CONCLUSIONS

Quantitative modeling of tracer concentration profiles obtained during double oxidation experiments has been carried out. The phenomenon of combined inward grain-boundary and lattice diffusion of oxygen with exchange has been modeled. The original model of Basu and Halloran[2] has been extended to incorporate the effects of variable grain size in the oxide for the case of inward oxygen diffusion. In this model, the spherical geometry of grains is retained due to the symmetry of the volume diffusion. This allows the exchange process to be treated as a 1D problem, thereby reducing the complexity of the numerical calculations. The model has been extended to predict the tracer profile in the entire oxide. A graphical user interface has been developed for easy comparison of simulated profiles with experimental data.

We have carried out simulation of profiles for test cases to ensure the accuracy of our complex computer program. We have also tested the sensitivity of the simulated profiles to variations in D^v, D^b, and grain-size variation. The results show that the normalized tracer profiles are sensitive to variations in D^b to a lesser extent as compared to similar variations in D^v. The results also show that incorporation of variable grain size leads to profiles that are very different from those obtained from a constant grain-size assumption, in agreement with observations of Bongartz and co-workers.[7] We have used our computer program to fit experimental profiles reported by Bongartz *et al.*[7] to obtain values of D^v and D^b.

[1] S. Mrowec, *An Introduction to the Theory of Metal Oxidation* (National Bureau of Standards and National Science Foundation, Washington, DC, 1982), p. 339.
[2] S. N. Basu and J. W. Halloran, Oxid. Met. **27**, 143 (1987).
[3] J. Jedlinski and G. Borchardt, Oxid. Met. **36**, 317 (1991).
[4] B. A. Pint, J. R. Martin, and L. W. Hobbs, Oxid. Met. **39**, 167 (1993).
[5] J. Jedlinski, Oxid. Met. **39**, 61 (1993).
[6] W. Wegener and G. Borchardt, Oxid. Met. **36**, 339 (1991).
[7] K. Bongartz, W. J. Quadakkers, J. P. Pfeiffer, and J. S. Becker, Surf. Sci. **292**, 196 (1993).
[8] W. J. Quadakkers, A. Elschner, W. Speier, and H. Nickel, Appl. Surf. Sci. **52**, 271 (1991).

[9] Yu. M. Mishin and G. Borchardt, J. Phys. III (France) **3**, 863 (1993).
[10] Yu. M. Mishin and G. Borchardt, J. Phys. III (France) **3**, 945 (1993).
[11] L. G. Harrison, Trans. Faraday Soc. **57**, 1191 (1961).
[12] H. Hindam and D. P. Whittle, Oxid. Met. **18**, 245 (1982).
[13] R. Prescott and M. J. Graham, Oxid. Met. **38**, 233 (1992).
[14] Y. Oishi and H. Ichimura, J. Chem. Phys. **71**, 2281 (1979).
[15] N. Birks and G. H. Meier, *Introduction to High Temperature Oxidation of Metals* (Edward Arnold, London, 1983).
[16] Due to the large number of variables, multiple superscripts and subscripts are used. In general, a variable V has the form ${}^{X}V_{Z}^{Y}$, where X refers to the axis [depth (y) or radial distance from grain center (ρ)], Y refers to location [grain boundary (b), grain (v or grn), or scale (tot)], and Z refers to oxygen species (16 or 18).
[17] J. Crank, *The Mathematics of Diffusion* (Oxford University, New York, 1967).
[18] N. Appanaagaari, M.S. thesis, Boston University, 1994.